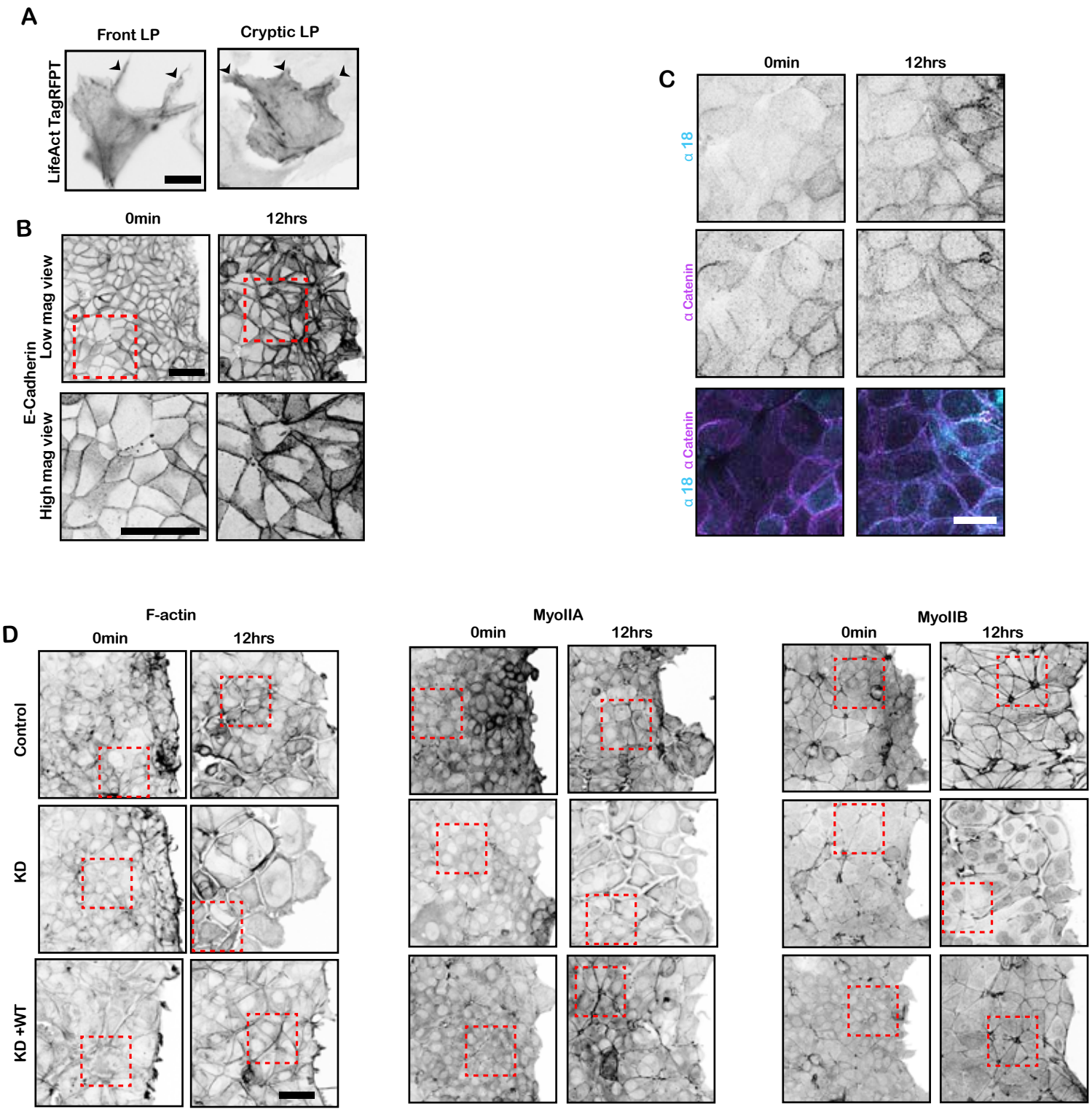


**Fig. S1. Characterization of MCF7 epithelial migration.**

(A) Fluorescence images showing active protrusions in cells expressing Lifeact-TagRFPT (arrowheads) at the leading margin and within the body (5-10 cell rows) of the migrating population. In the second case, cells surrounding the highlighted cells are identified by low level expression of LifeAct. Scale bar: 20µm.

(B) E-cadherin staining in migrating MCF7 cells. Higher magnification views are taken from the boxed regions.

(C) α-18 mAB and α-catenin staining: single channel images and overlays (corresponding to Fig 1D).

(D) Low magnification views of F-actin and Myosin IIA and IIB in migrating MCF7 cells (corresponding to Fig 1E-G, identified by boxes).

Scale bars: (B,D) 50µm (C) 20µm.

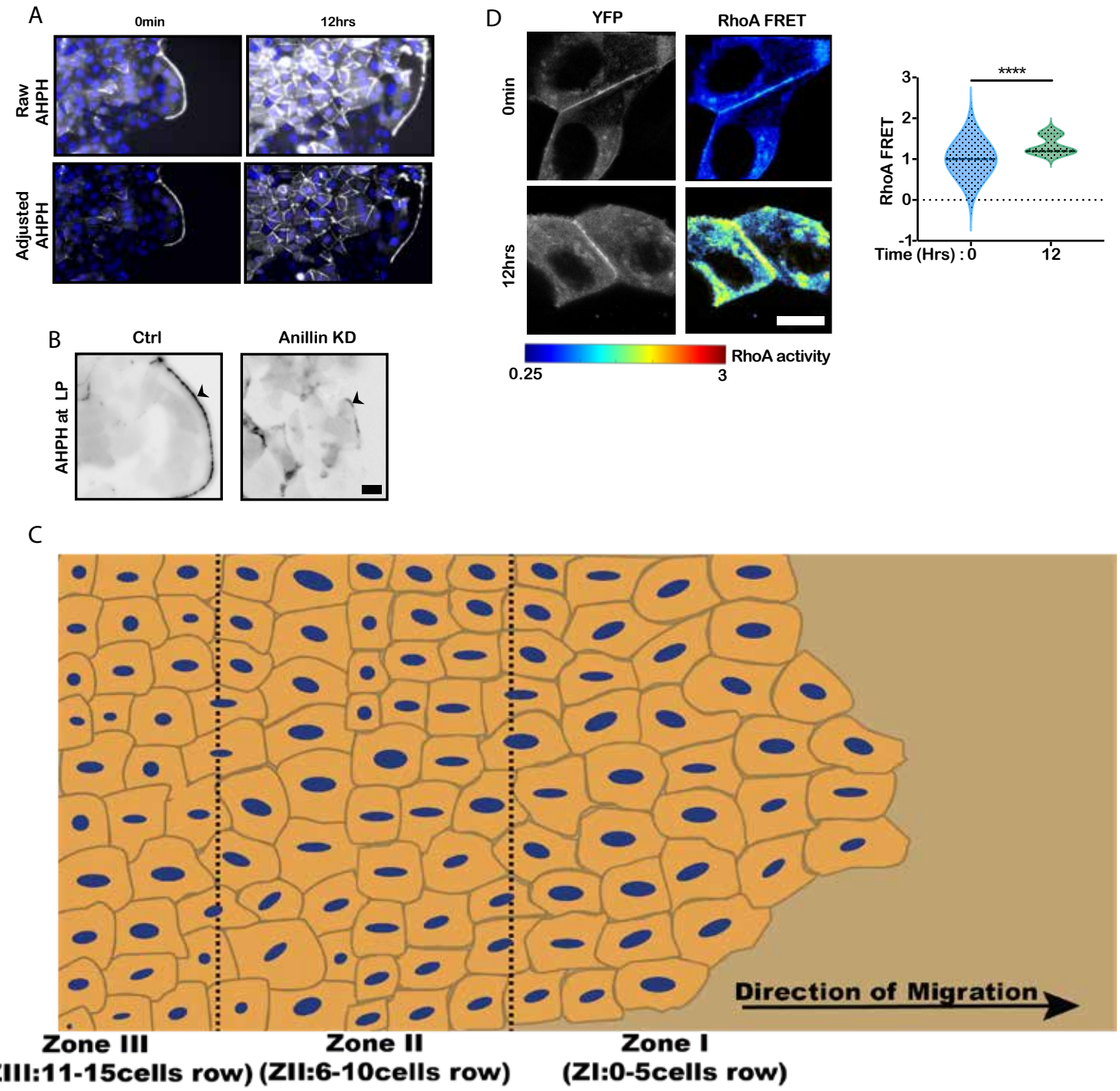


**Fig. S2. Active GTP-RhoA levels and localisation.**

(A) Fluorescence images showing raw and intensity-adjusted AHPH images at 0 min and 12 hours post migration.
(B) AHPH localisation in lamellipodia of leader cells in both Control and Anillin KD cultures.
(C) Diagram of zones that are used for quantification analysis.
(D) Change in junctional RhoA activation during MCF-7 monolayer migration measured using a FRET-based activity sensor. YFP and RhoA FRET (CFP/YFP) emission ratios images measured at ZA of cells during CCM. Cells analysed were in the first 7 rows of cells. The graph shows an increase in RhoA FRET index after 12 hours of migration.
Data are means ± SEM; n=3 independent experiments (each comprising 18-22 technical replicates). ****,P<0.0009; unpaired t-test. Scale bar: (B) 20µm (D) 10µm.

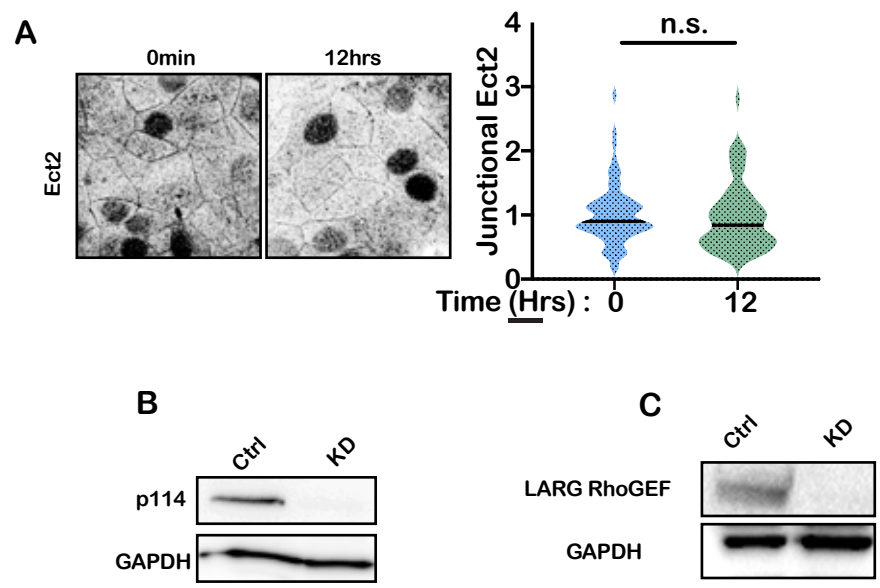


**Fig. S3. Analysis of GEFs in epithelial migration.**

(A) Immunostaining for Ect2 during MCF7 migration. Representative images and quantitation of junctional staining were performed on cells in the first 7 rows of the monolayer. Scale Bar: 20μm. Data are means ± SEM; n=3 independent experiments (each comprising 18-22 technical replicates). ns: non-significant.
(B,C) Western blots for depletion by RNAi of p114 RhoGEF (B) and LARG (C).

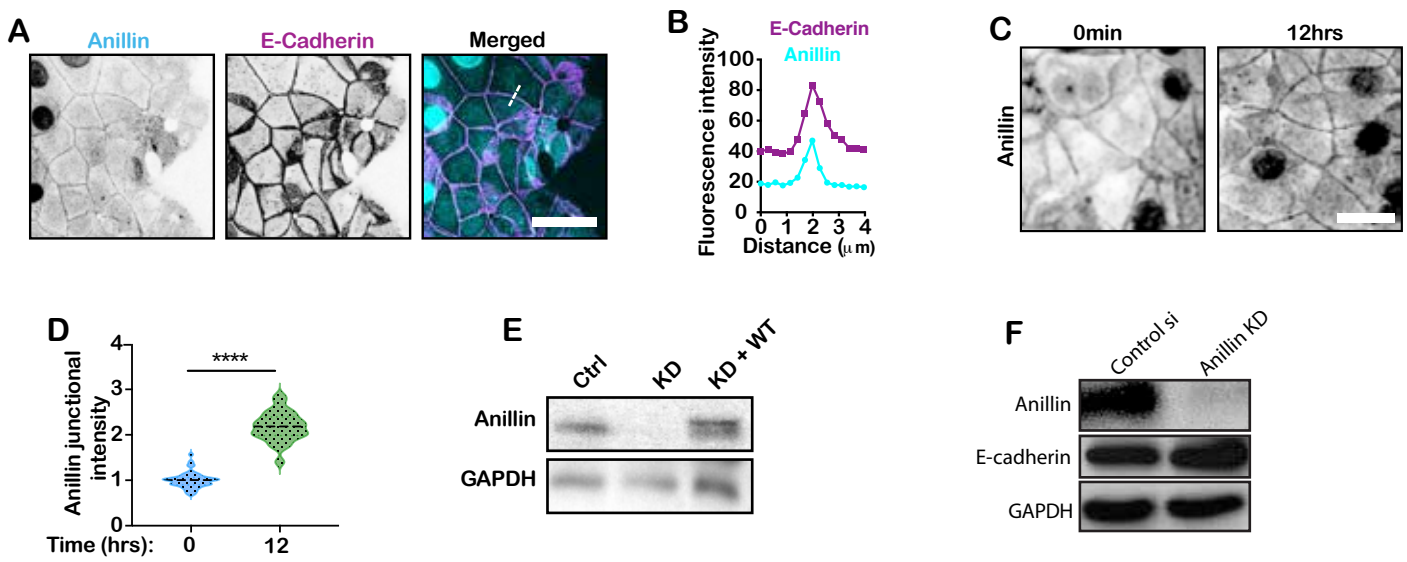


## Fig. S4. Anillin in monolayer migration.

(A,B) Colocalization of anillin with E-cadherin in a representative migrating monolayer: immunofluorescence images (A) and quantitative comparison by line scan analysis (B).(C,D) Anillin increases at AJ in migrating MCF-7 monolayers: representative images (C) and quantification (D) taken within the first 7 rows of cells.
(E) Western analysis for RNA-based depletion of anillin and expression of an RNAi-resistant wild-type (WT) transgene.
(F) Western analysis of E-cadherin expression in control and Anillin RNAi monolayers.
Data are means ± SEM; n=3 independent experiments (each comprising 18-22 technical replicates). ****,P<0.0009; unpaired t-test. Scale bars: A,C: 20μm

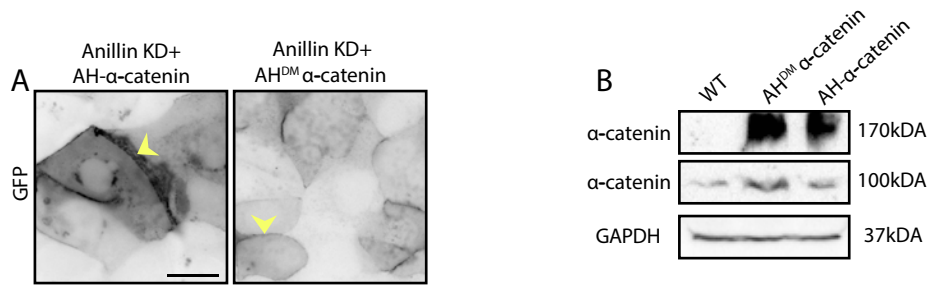


**Fig. S5. Expression of chimeric AH-α-catenin transgene.**
Localization at cell-cell junctions identified by the GFP tag (A, arrowheads) and cellular expression characterized by Western analysis (B).

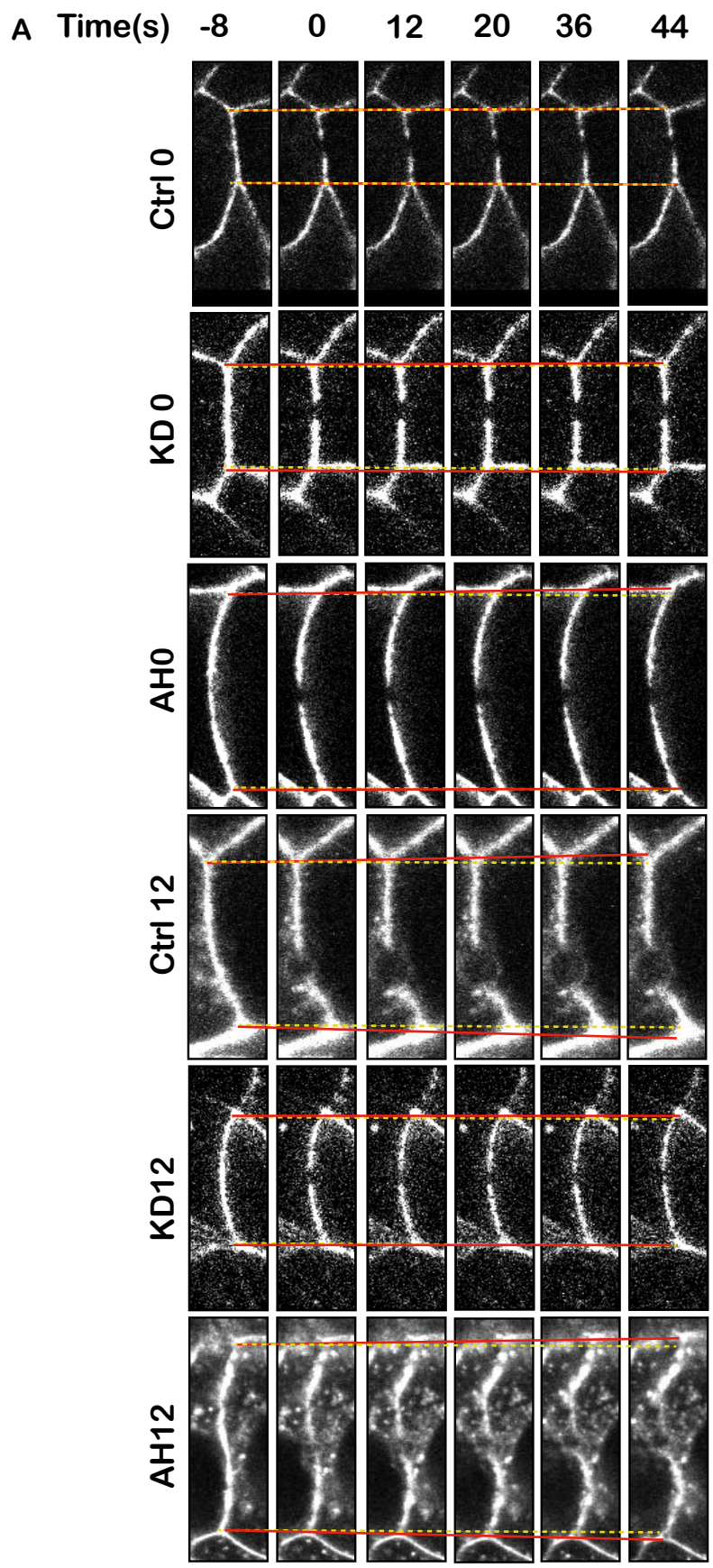


**Fig. S6. Recoil of junctional vertices after laser ablation**.
Representative montages from recoil movies (frames -8 to +44 sec relative to the ablation) taken at 0 hr and 12 hr of migration. Cultures were controls (Ctr), anillin KD (KD) and KD cells reconstituted with AH-α-catenin (AH).

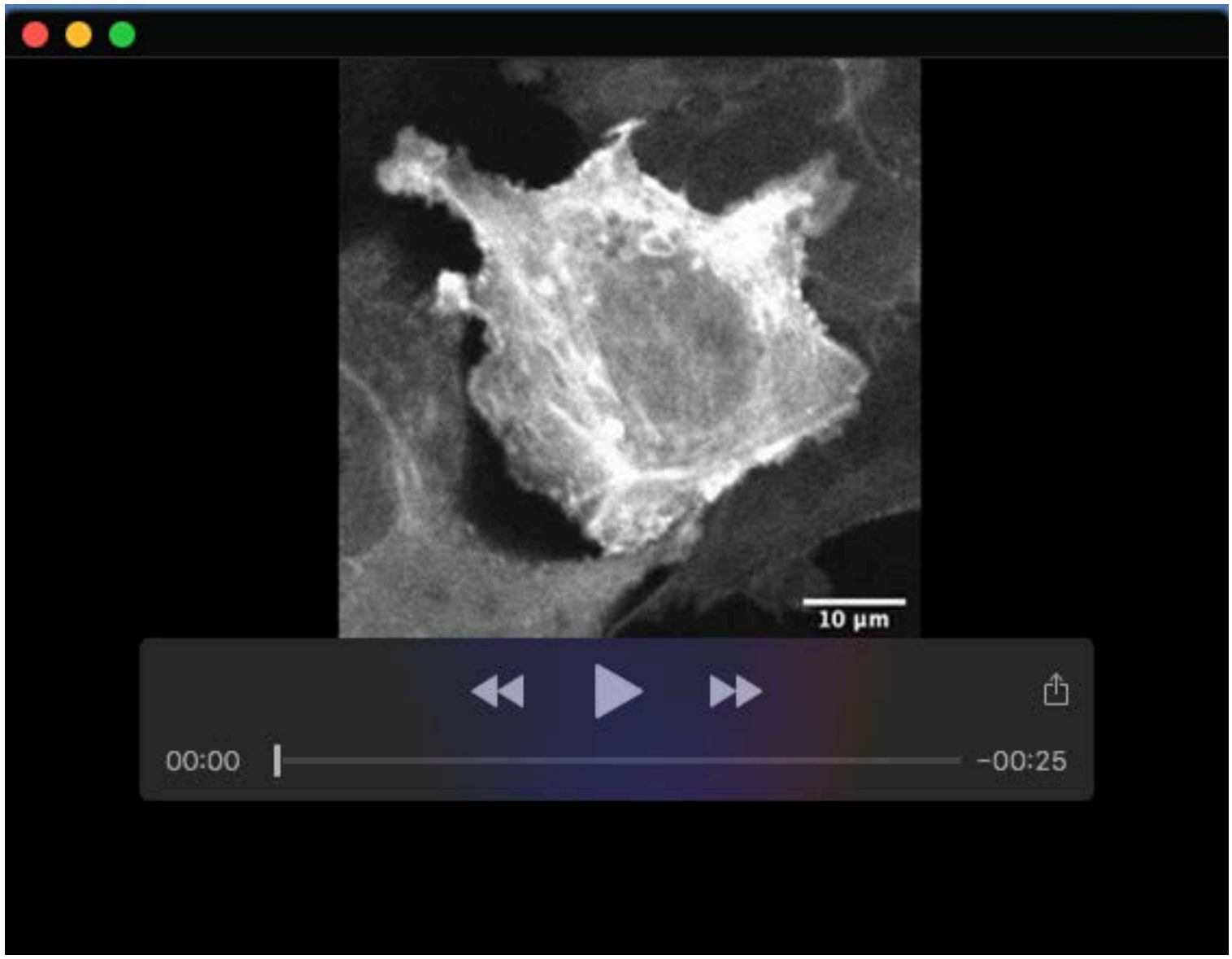


**Movie 1.** Cryptic lamellipodia within the migrating sheet.

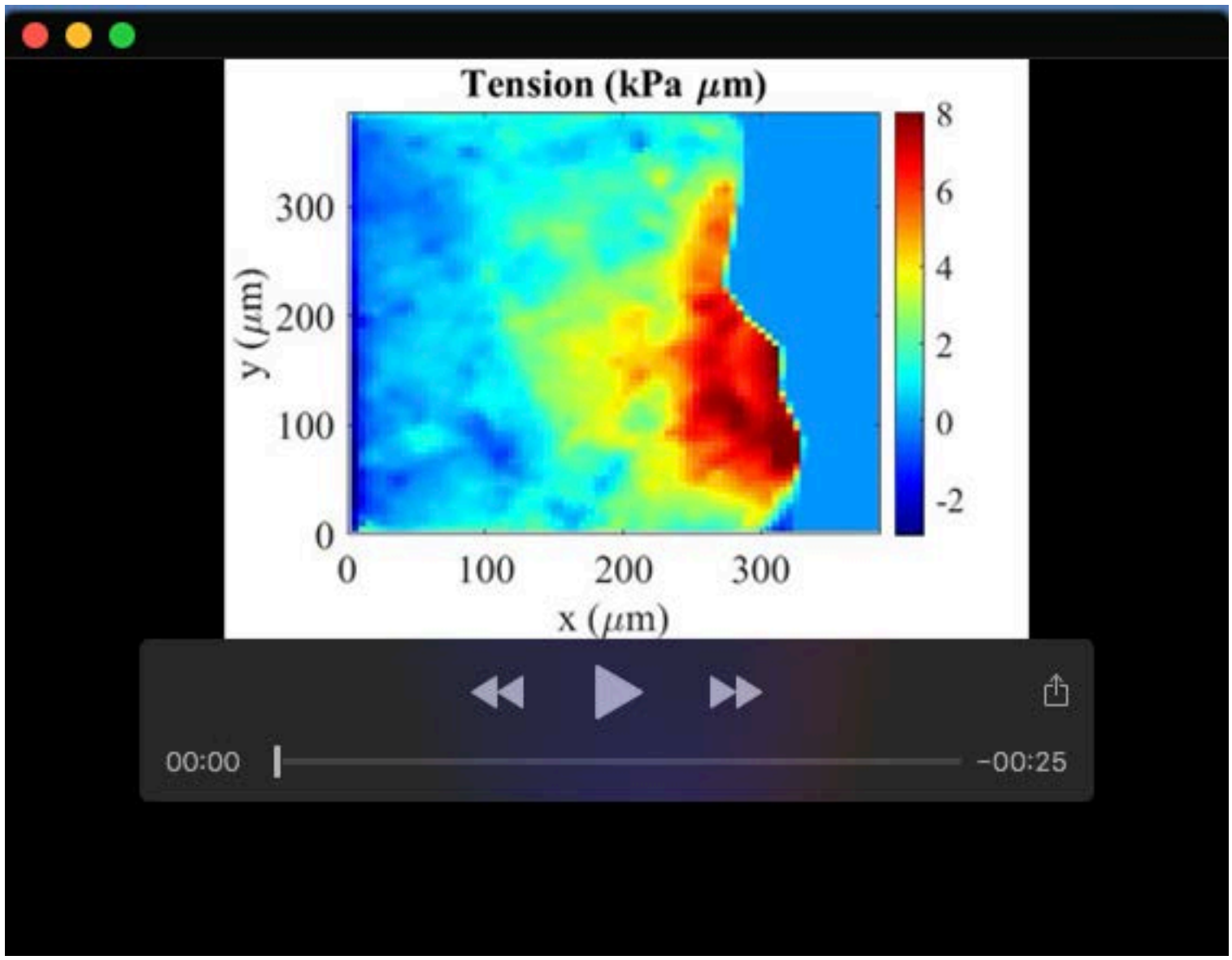


**Movie 2.** Monolayer stress inferred by Bayesian Inversion Stress Microscopy during migration.


**Movie 3.** AHPH levels at cell junctions increased significantly when cells began to move collectively.

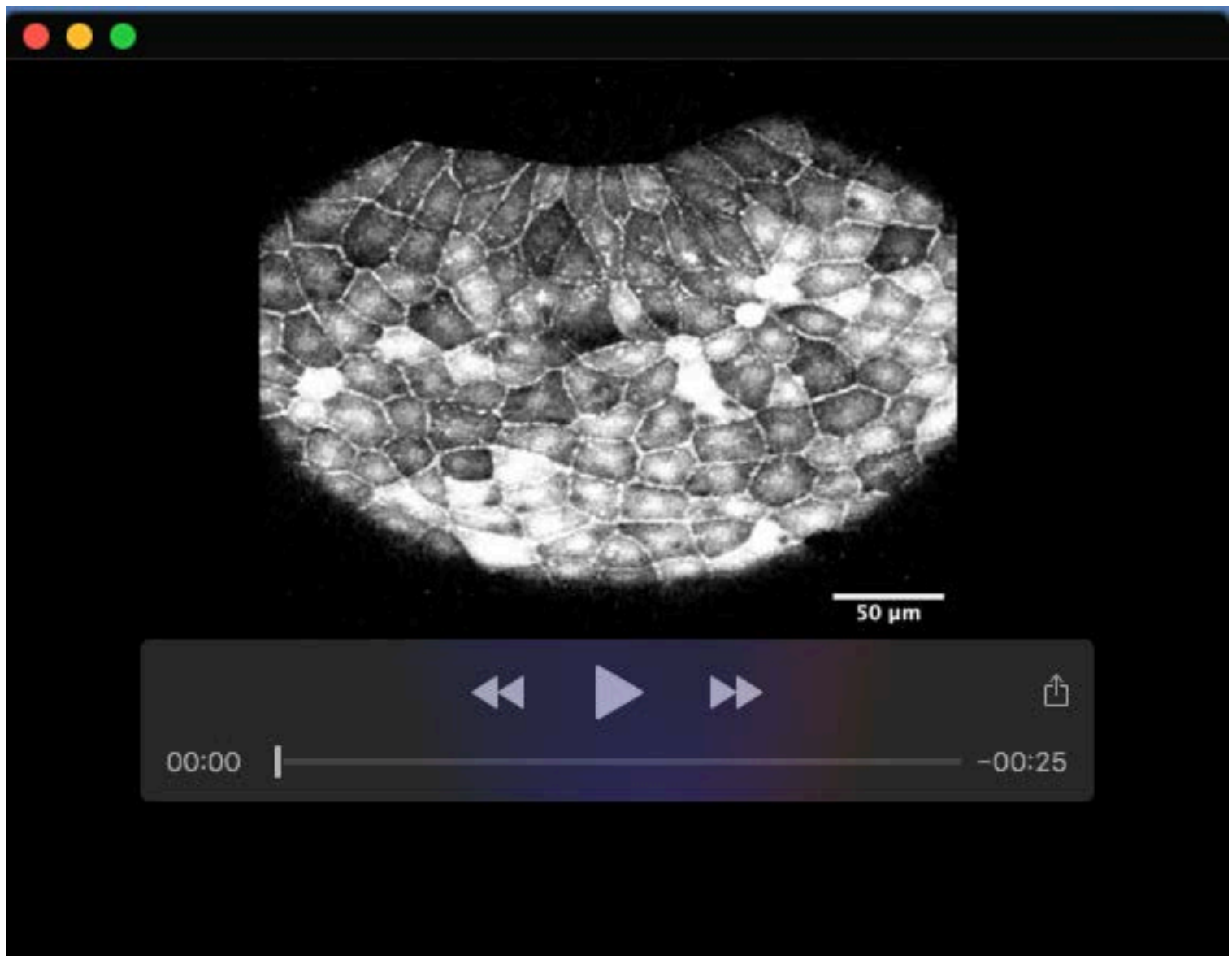


**Movie 4.** AHPH level increases during the progression of epiboly in Zebrafish.